Static and Dynamic Aspects of Voltage-Power relationships in Electric Power Systems

Stephen R. Fernandes[1]

[1]Department of Electrical Engineering, Petrofac Engineering India Ltd., Mumbai, India; formerly a Ph.D candidate at the University of Illinois at Urbana-Champaign, Illinois, USA.

Abstract: *This paper investigates various aspects of voltage-power relationships in power systems. Conditions for feasible generating points are analytically derived for a simple power system with a detailed generator model. The set of Hopf Bifurcation points for the sample system are visualized on the feasible operating surface. The effect of damping on the onset of bifurcations in the system is briefly investigated. The role of different generator models in isolating bifurcations and subsidiary phenomena in a multi-machine system are also presented. The effect of nonlinear indices of voltage dependent load models on system bifurcations is dealt with as also the effect of AVR gains.*

Keywords - *Steady-state Stability, bifurcations, critical eigenvalues, P-V curves.*

I. INTRODUCTION

Power Systems are large complex dynamical systems. The nature of voltage-power relationships at any bus within such systems likewise varies in a complex manner depending on where and how the system is stressed, where the generating nodes are, network parameters and a host of other factors. Deriving explicit expressions for such complex voltage-power behaviour at any bus in a stressed system is too intricate. However, power system researchers have visualized such relationships using power-voltage (PV) curves constructed using detailed power system models.

Power voltage curves have as such long been visualized and used in the analysis for various phenomena in stressed power systems including structural stability, voltage instability, bifurcations etc. ([2]-[5]). The dynamic aspects of such voltage power characteristics have also been studied in detail ([2]-[4]). Dynamic models of power systems coupled with P-V curves present the researcher with tools to analyze both static and dynamic aspects of power systems. However, it is interesting to note that the amount of detail used in constructing dynamic system models is crucial in highlighting phenomena which usually cannot be visualized in reduced order models. Adequate load modeling at different buses also play an important role in predicting the occurrence of such dynamic phenomena.

This paper discusses the static and dynamic aspects of voltage-power characteristics in two sample power systems. The onset of dynamic phenomena such as Hopf bifurcations is visualized using voltage-power characteristics at a load bus. The effect of different detailed models on defining the onset of such phenomena is investigated. The nature of different static load models, their power-voltage characteristics, their sensitivities with respect to voltage variations and their effect on the occurrence of Hopf bifurcations is also investigated. The effect of AVR gain Ka on the onset of such dynamic phenomena is also briefly dealt with.

II. SYSTEM DYNAMIC MODEL

A simple power system consisting of a single generator synchronized on an infinite bus through a lumped transmission line, as shown in Fig. 1, is analyzed. The generator is modeled by a two axis machine model with IEEE Type 1 exciter and a simplified turbine-governor model. The saturation effects in the generator along with both stator and network transients are neglected. The synchronous machine equations are:

$$\frac{d\delta}{dt} \;=\; \omega - \omega_S \tag{2.1}$$

$$\frac{d\omega}{dt} \;=\; \frac{T_M}{M} \;-\; \frac{\left[E'_q - X'_d I_d\right]I_q}{M} \;-\; \frac{\left[E'_d + X'_q I_q\right]I_d}{M} \;-\; \frac{D\left(\omega - \omega_S\right)}{M} \tag{2.2}$$

$$\frac{dE'_q}{dt} \;=\; -\,\frac{\left(E'_q\right)}{T'_{do}} \;-\; \frac{(X_d - X'_d)I_d}{T'_{do}} \;+\; \frac{\left(E_{fd}\right)}{T'_{do}} \tag{2.3}$$

$$\frac{dE'_d}{dt} \;=\; -\,\frac{\left(E'_d\right)}{T'_{qo}} \;+\; \frac{I_q\left(X_q - X'_q\right)}{T'_{qo}} \tag{2.4}$$

$$V \, \varepsilon^{j\theta} \quad = \quad \left(V_d + j \, V_q\right) \varepsilon^{j\left(\delta - \frac{\pi}{2}\right)}$$

$$V_\infty \, \angle 0$$

$$I_D + j \, I_Q = \left(I_d + j \, I_q\right) \varepsilon^{j\left(\delta - \frac{\pi}{2}\right)}$$

$$\left[E'_d + \left(X'_q - X'_d\right) I_q + j \, E'_q\right] \varepsilon^{j\left(\delta - \frac{\pi}{2}\right)}$$
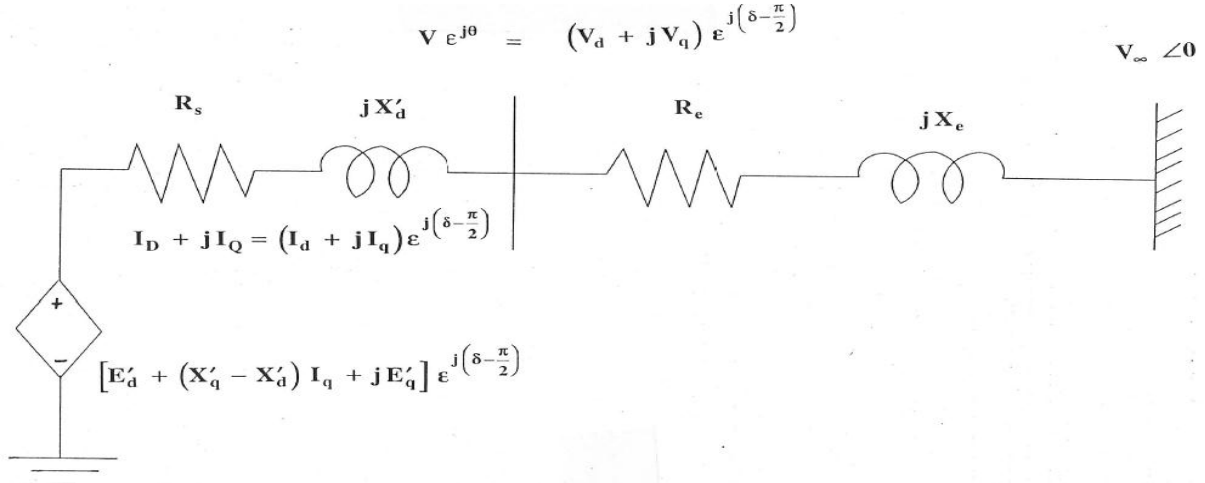
Fig. 1 Single Machine Infinite Bus System

The IEEE Type I exciter dynamics are given by:

$$\frac{dE_{fd}}{dt} \quad = \quad - \quad \frac{K_E + S_E\left(E_{fd}\right)}{T_E}\left(E_{fd}\right) \quad + \quad \frac{\left(V_R\right)}{T_E} \tag{2.5}$$

$$\frac{dV_R}{dt} \quad = \quad - \quad \frac{\left(V_R\right)}{T_A} \quad + \quad \frac{K_A}{T_A}\left(R_F\right) \quad - \quad \frac{K_A K_F}{T_A T_F}\left(E_{fd}\right) \quad + \quad \frac{K_A}{T_A}\left(V_{ref} - V\right) \tag{2.6}$$

$$\frac{dR_F}{dt} \quad = \quad - \quad \frac{\left(R_F\right)}{T_F} \quad + \quad \frac{K_F}{T_F^2}\left(E_{fd}\right) \tag{2.7}$$

where V_{ref} is a set point and V is the magnitude of the generator terminal voltage. The simplified turbine and governor model is given by:

$$\frac{dT_M}{dt} \quad = \quad - \quad \frac{\left(T_M\right)}{T_{RH}} \quad + \quad \left(\frac{1}{T_{RH}} - \frac{K_{HP}}{T_{CH}}\right)\left(P_{CH}\right) \quad + \quad \frac{K_{HP}}{T_{CH}}\left(P_{SV}\right) \tag{2.8}$$

$$\frac{dP_{CH}}{dt} \quad = \quad - \quad \frac{\left(P_{CH}\right)}{T_{CH}} \quad + \quad \frac{\left(P_{SV}\right)}{T_{CH}} \tag{2.9}$$

$$\frac{dP_{SV}}{dt} \quad = \quad - \quad \frac{\left(P_{SV}\right)}{T_{SV}} \quad + \quad \frac{P_C}{T_{SV}} \quad - \quad \frac{1}{R_d T_{SV}}\left(\frac{\omega}{\omega_S} - 1\right) \tag{2.10}$$

In the above model, $S_E\left(E_{fd}\right) = A_{ex} \varepsilon^{B_{ex}\left(E_{fd}\right)}$ models the saturation in the exciter and $M = 2H/\omega_S$, $\omega_S = 120\pi$ rads/sec. The following limit constraints also apply to the model

$$V_R^{min} \le \left(V_R\right) \le V_R^{max} \qquad \text{and} \qquad 0 \le \left(P_{Sv}\right) \le P_{SV}^{max} \tag{2.11}$$

The stator algebraic equations to be satisfied are:

$$\left(E'_d\right) - V \sin(\delta - \theta) - R_S I_d + X'_q I_q = 0 \tag{2.12}$$

$$\left(E'_q\right) - V \cos(\delta - \theta) - R_S I_q - X'_d I_d = 0 \tag{2.13}$$

For the single machine infinite bus case the network equations to be satisfied are :

$$R_e I_d - X_e I_q - V \sin(\delta - \theta) + V_\infty \sin(\delta) = 0 \tag{2.14}$$

$$X_e I_d + R_e I_q - V \cos(\delta - \theta) + V_\infty \cos(\delta) = 0 \tag{2.15}$$

The differentio-algebraic model illustrated above can be symbolically represented as :

$$\dot{X} = f(X, Y, p) \tag{2.16}$$

$$0 = g(X, Y, p) \tag{2.17}$$

where X is the vector containing all differential states, Y is the vector containing all algebraic states and p is the vector of all system parameters. The above model can be linearized about an equilibrium point. The symbolic representation of the perturbation model has the form:

$$\Delta \dot{X} = A\,\Delta X + B\,\Delta Y + E\,\Delta p \tag{2.18}$$

$$0 = C\,\Delta X + D\,\Delta Y + F\,\Delta p \tag{2.19}$$

where
$$A = \frac{\partial f}{\partial X} \quad,\quad B = \frac{\partial f}{\partial Y} \quad,\quad E = \frac{\partial f}{\partial p}$$
$$C = \frac{\partial g}{\partial X} \quad,\quad D = \frac{\partial g}{\partial Y} \quad,\quad F = \frac{\partial g}{\partial p}$$

and $\Delta X, \Delta Y$ denote perturbation in the differential and algebraic states, Δp denotes perturbation in system parameters. Eliminating ΔY from equations (2.18) and (2.19) we have the following representation:

$$\Delta \dot{X} = A_{SYS}\,\Delta X + G\,\Delta p \tag{2.20}$$

where $A_{SYS} = \left(A - BD^{-1}C\right),\ \ G = \left(E - BD^{-1}F\right).$ The eigenvalues to be observed are the eigenvalues of the A_{SYS} matrix.

III. FEASIBLE GENERATING SET

The network algebraic equations (2.14) and (2.15) of the single machine infinite bus system model outlined in section 2 are derived from the following equation satisfying Kirchoff's voltage law in the network:

$$V\varepsilon^{j\theta} - \left(I_d + jI_q\right)\varepsilon^{j\left(\delta-\frac{\pi}{2}\right)}\left(R_e + jX_e\right) = V_{\infty}\varepsilon^{j0} \tag{3.1}$$

The complex generated power at the generator bus is given by:

$$P_G + jQ_G = V\varepsilon^{j\theta}\left(I_d - jI_q\right)\varepsilon^{-j\left(\delta-\frac{\pi}{2}\right)} \tag{3.2}$$

Using (3.2) we can eliminate the currents I_d, I_q from (3.1) which then can be written as:

$$V\varepsilon^{j\theta} - \frac{\left(P_G - jQ_G\right)}{V\varepsilon^{-j\theta}}\left(R_e + jX_e\right) = V_{\infty}\varepsilon^{j0} \tag{3.3}$$

or
$$V^2 - \left(P_G - jQ_G\right)\left(R_e + jX_e\right) = V\varepsilon^{-j\theta}\,V_{\infty}\varepsilon^{j0} \tag{3.4}$$

Separating (3.4) into real and imaginary components and taking $V_{\infty} = 1$ p.u we have:

$$V^2 - V\cos\theta - a = 0 \tag{3.5}$$

$$V\sin\theta - b = 0 \tag{3.6}$$

where $a = P_G R_e + Q_G X_e$, $b = P_G X_e - Q_G R_e$. Eliminating θ from (3.5) and (3.6) we have the following equation which can be solved for V

$$V^2 \mp \sqrt{V^2 - b^2} - a = 0 \tag{3.7}$$

Multiplying the two equations corresponding to each of the two different signs in (3.7) we have:

$$V^4 - \left(2a+1\right)V^2 + a^2 + b^2 = 0 \tag{3.8}$$

Two of the four solutions of (3.8) will correspond to two solutions of each of the two equations forming it. Substituting $q = V^2$ in (3.8) we have:

$$q^2 - \left(2a+1\right)q + a^2 + b^2 = 0 \tag{3.9}$$

which has two roots

$$q_{1,2} = \frac{\left(2a+1\right) \pm \sqrt{\left(2a+1\right)^2 - 4\left(a^2 + b^2\right)}}{2} \tag{3.10}$$
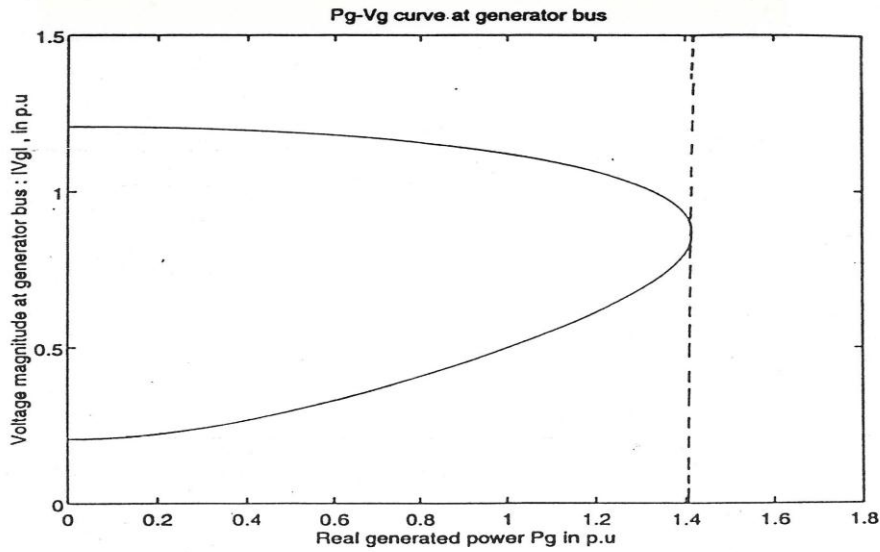
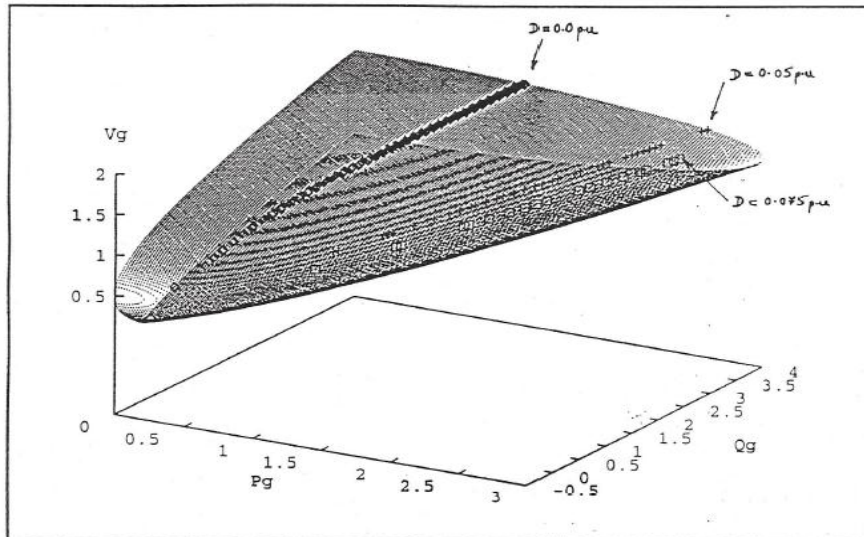Fig 2a $P_G - V$ for $Q_G = 0.5$ p.u for the infinite bus system

Fig 2b 3-Dimensional surface of feasible generating points for the infinite bus system

The two roots in (3.10) can be (a) both real and ≥ 0 or both real and ≥ 0 or (b) both imaginary with real parts the same, depending on the term inside the square root being (i) ≥ 0 or (ii) < 0 respectively. When the two solutions for q given by (3.10) are both real and < 0 or both imaginary then the four solutions for V in (3.8) are guaranteed to be all imaginary leading to a loss of a feasible solution. Both solutions for q in (3.10) are negative when

$$2a + 1 < 0 \quad \text{or} \quad a < -1/2 \tag{3.11}$$

Both solutions of q in (3.10) are imaginary when

$$(2a+1)^2 - 4(a^2 + b^2) < 0 \quad \text{or} \quad 4b^2 - 4a - 1 > 0$$

$$\Rightarrow \quad |b| > \sqrt{a + 1/4} \tag{3.12}$$

Consider again (3.7). The Jacobian of the L.H.S of (3.7) yields

$$J = V\left(2 \mp \frac{1}{\sqrt{V^2 - b^2}}\right) \tag{3.13}$$

J^{-1} fails to exist when V=0 which is a trivial solution or when

$$2 \mp \frac{1}{\sqrt{V^2 - b^2}} = 0 \implies V = \pm \sqrt{b^2 + 1/4} \tag{3.14}$$

The critical value of generator terminal voltage can thus be derived by substituting the critical value of b from (3.12) into (3.14) which gives:

$$V_C = \sqrt{b_C^2 + 1/4} = \sqrt{a^2 + 1/2} \tag{3.15}$$

From (3.11),(3.12) and (3.15) the set of all feasible generating points for the single machine infinite bus system can be constructed as shown in Fig. 2b for a lossless line. The 3-dimensional feasible operating surface is a conglomeration of all P_G vs V curves of the form shown in Fig. 2a (for $Q_G = 0.5$ p.u), for all Q_G within the desirable operating range. The locus of all operating points (where loss of existence of a feasible solution occurs) can be found by joining the tip of all P_G vs V curves for different Q_G in the desired range.

IV. BIFURCATION ANALYSIS

For the system (2.16)-(2.17) with perturbation model given by (2.20), conditions for Hopf bifurcation to occur are (a) a simple pair of imaginary eigenvalues of A_{SYS} matrix cross the imaginary axis while the other (n-2) eigenvalues are all in the left half plane and

$$\text{(b)} \qquad \frac{d}{dp_j}\left(\text{Re}\left(\lambda\left(p_j\right)\right)\right)\Bigg|_{p_j = p_{jC}} \neq 0 \tag{4.1}$$

that is, the rate of change of the real part of the critical pair of eigenvalues with variation of the jth parameter p_j, is nonzero at the point where the critical parameter $p_j = p_{jC}$. In the feasible generating space shown in Fig. 2b, the set of Hopf bifurcating points are isolated using the above criteria and the results shown in Fig. 2b. The Hopf Bifurcating locus is plotted only for the upper part of the feasible operating surface that is only when the critical eigenvalues move over from the left half to the right half of the complex plane. Increased damping D, in equation (2.2), in the system causes the Hopf bifurcation locus to shift lower down the feasible operating surface till for some value of damping the locus vanishes and the upper part of the feasible operating surface ceases to have Hopf Bifurcation points beyond that critical damping. A critical value exists too when damping D becomes negative in the model. To verify that the above linearized analysis is actually coherent with nonlinear time domain simulation, three different feasible operating points in the feasible operating surface were chosen as shown in Table 1.

The system was perturbed from these operating points and the nonlinear model was simulated using the Simultaneous Implicit Trapezoidal Method with a constant time step of 0.005 sec. The results for each case are as shown in Fig. 3. The system is stable for case (a), exhibits periodic cycles for case (b) which is the Hopf bifurcation point under study and is constrained to exhibit supercritical bifurcation like phenomena for case(c) depicting a realistic scenario.
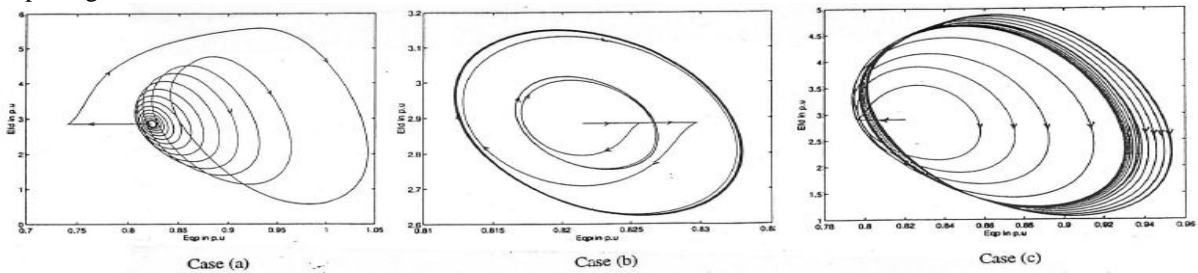

Fig. 3 Nonlinear Simulation of the SMIB system around the Hopf Bifurcation point

V. MULTIMACHINE SYSTEMS

The system model for a multimachine system is represented by a set of machine models each of the form (2.1)-(2.11), along with the associated stator algebraic equations of the form (2.12)-(2.13) with parameters in the above equations corresponding to each machine in the system. The set of network equations derived by applying Kirchoff's voltage laws to the system network are: (assuming an n bus system with m generators synchronized on the first m network buses)

$$I_{d_i}V_i \sin(\delta_i - \theta_i) + I_{q_i}V_i \cos(\delta_i - \theta_i) + P_{L_i}(V_i) - \sum_{k=1}^{n} V_i V_k Y_{ik} \cos(\theta_i - \theta_k - \alpha_{ik}) = 0 \tag{5.1}$$

$$I_{d_i}V_i \cos(\delta_i - \theta_i) - I_{q_i}V_i \sin(\delta_i - \theta_i) + Q_{L_i}(V_i) - \sum_{k=1}^{n} V_i V_k Y_{ik} \sin(\theta_i - \theta_k - \alpha_{ik}) = 0 \quad i = 1, \ldots, m \tag{5.2}$$

$$P_{L_i}(V_i) - \sum_{k=1}^{n} V_i V_k Y_{ik} \cos(\theta_i - \theta_k - \alpha_{ik}) = 0 \tag{5.3}$$

$$Q_{L_i}(V_i) - \sum_{k=1}^{n} V_i V_k Y_{ik} \sin(\theta_i - \theta_k - \alpha_{ik}) = 0 \quad i = m+1, \ldots, n \tag{5.4}$$

where $P_{Li}(V_i)$, $Q_{Li}(V_i)$ denote voltage dependent exponential load models at the ith bus.

TABLE 1

Case	$P_G + jQ_G$	*Critical Eigenvalue Pair*
(a)	1.14 + j 0.2	- 0.2028 $\pm$ j 4.7868 in L.H.P
(b)	1.14637 + j 0.2	0.0000 $\pm$ j 4.4518 at Hopf Bif.
(c)	1.15 + j 0.2	+ 0.1523 $\pm$ j 4.3125 in R.H.P

The three machine nine bus Western System Coordinating Council (WSCC) system shown in Fig. 4 with model parameters as given in [6] is chosen for analysis in this section. Four different generator models are used to study the role of bifurcations in this system. The generator models chosen are:
(a) Model-A: Two-axis model with IEEE Type I exciter; same as outlined in section 2.
(b) Model-B: Flux decay model with fast exciter. The damper winding constants in model (a) are assumed to be very small and are set to zero which in essence means that an integral manifold exists for these states. Equation (2.4) can then be written as:

$$0 = -E'_d + (X_q - X'_q)I_q \tag{5.5}$$

We use equation (5.5) to eliminate E'_d from equations (2.4) and (2.12). The exciter is modeled

by one dynamic equation:

$$\frac{dE_{fd}}{dt} = -\frac{E_{fd}}{T_A} + \frac{K_A}{T_A}(V_{ref} - V) \tag{5.6}$$

(c) Model C: Two-axis model with fast exciter. The model is essentially the same as in (a) except that the single exciter equation (5.6) replaces the set of three equations representing the IEEE Type I exciter.
(d) Model D: Flux decay model with IEEE Type I exciter. The generator model is the same as in case (b) but the exciter is IEEE Type I with three dynamic equations, (2.5)-(2.7). For convenience, the turbine-governor dynamics are not modeled in any of the above. The zero eigenvalue inherent in such models is removed by introducing relative rotor angles.
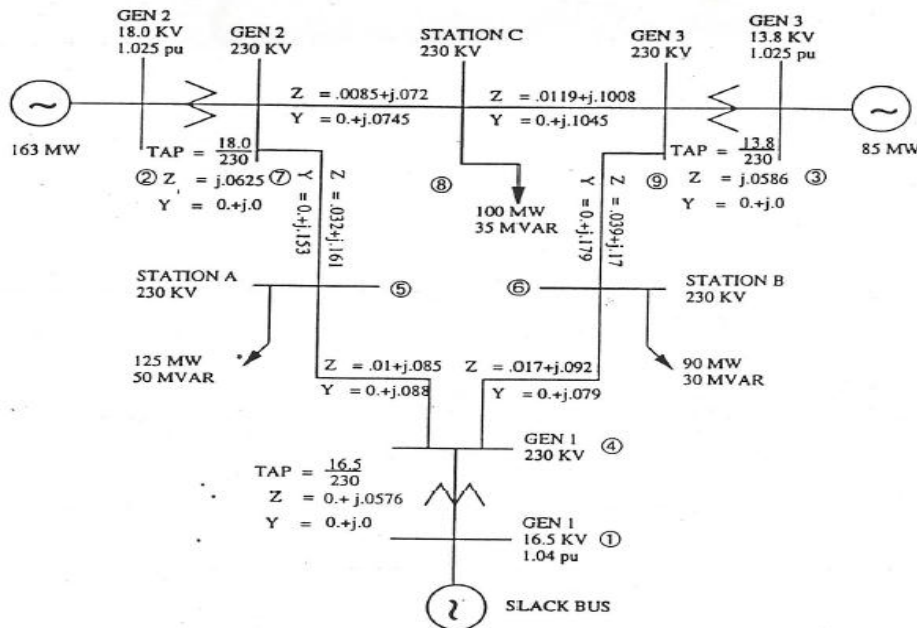

Fig. 4 WSCC 3 machine 9 bus system

VI.   STATIC LOAD MODELS

Loads are a part of every power system and their characteristics do affect the dynamic behaviour of such systems. So, when power networks are modeled for analysis effective load modeling becomes an essential step in the process. Past literature ([7]-[12]) abounds in different modeling aspects of static and dynamic load models.

Effective load models as such, should be realistic, simple and strike a proper balance among the different load mixes existing in the actual system. Such load mix composition modeling requires reliable estimation. Since, there is always an element of uncertainty in such estimation, prevalent load models are inherently conservative by design. In this analysis presented here we stick to the generic load models which have been presented in literature, more precisely we consider only voltage dependent exponential load models of the form:

$$S_{L_i} = P_{L_i} + jQ_{L_i} \qquad \text{at the ith bus where}$$

$$P_{L_i} \;=\; P_{0_i}\left(\frac{V_i}{V_{0_i}}\right)^{np_i} \quad , \quad Q_{L_i} \;=\; Q_{0_i}\left(\frac{V_i}{V_{0_i}}\right)^{nq_i} \tag{6.1}$$

The load-voltage characteristics for such load models are as shown in Fig. 5(a)-(b) for different nonlinear load indices. The endeavour in this and subsequent sections is to investigate the nature of voltage sensitivities of such generic load models in an effort to visualize what effects such characteristics have on system stability and on the onset of bifurcations when carrying out a dynamic analysis of power systems using power-voltage curves at a

critical load bus. Consider the exponential real load model approximation at the ith bus: $P_{L_i} = P_{0_i}\left(\dfrac{V_i}{V_{0_i}}\right)^{np_i}$ with

operating constraints (relaxed) : $V \geq 0$, $np_i \geq 0$, $P_{0_i} \geq 0$. The voltage sensitivity of P_{L_i} is given by:

$$\frac{\partial P_{L_i}}{\partial V_i} \;=\; np_i\,\frac{P_{0_i}}{\left(V_{0_i}\right)^{np_i}}\,V^{np_i-1} \;=\; np_i\left(\frac{P_{L_i}}{V_i}\right) \tag{6.2}$$

The sensitivity of P_{L_i} with respect to np_i can be written as:

$$\frac{\partial P_{L_i}}{\partial np_i} \;=\; P_{0_i}\left(\frac{V_i}{V_{0_i}}\right)^{np_i}\ln\left(\frac{V_i}{V_{0_i}}\right) \;=\; P_{L_i}\ln\left(\frac{V_i}{V_{0_i}}\right)$$

Further

$$\frac{\partial^2 P_{L_i}}{\partial V_i^2} \;=\; np_i.(np_i-1)\,P_0\,\frac{V_i^{np_i-2}}{V_{0_i}^{np_i}} \;=\; np_i(np_i-1)\left(\frac{P_i}{V_i^2}\right) \tag{6.4}$$

And

$$\frac{\partial^2 P_{L_i}}{\partial V_i^2} > 0 \;\; \text{if}\;\; np_i > 1, \;\; \leq 0 \;\; \text{if}\;\; np_i \leq 1$$

This implies that the voltage sensitivity of the load follows the variation in voltage for $np_i > 1$ (namely increases with increasing voltage or vice versa), remains constant for $np_i = 1$ and changes in the opposite direction for $np_i < 1$ (namely decreases with increasing voltage). For the load-voltage sensitivity to be a constantly increasing function of the load index we then have (rate of change of voltage sensitivity with load index should be positive):
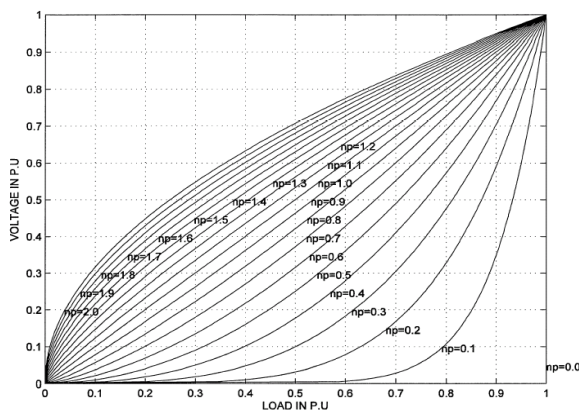

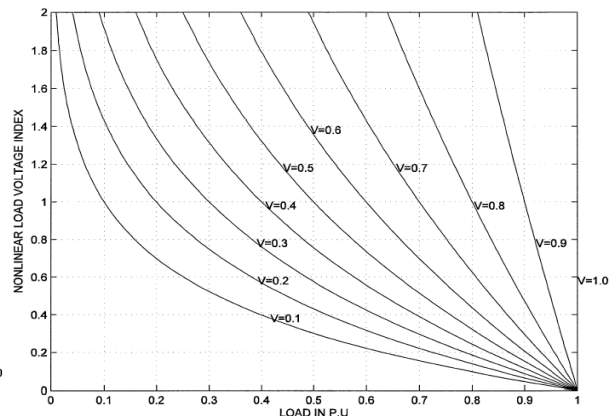Fig. 5a. Voltage Dependent Load Vs Voltage for varying Indices   Fig. 5b Voltage dependent load vs Indices for varying Voltage
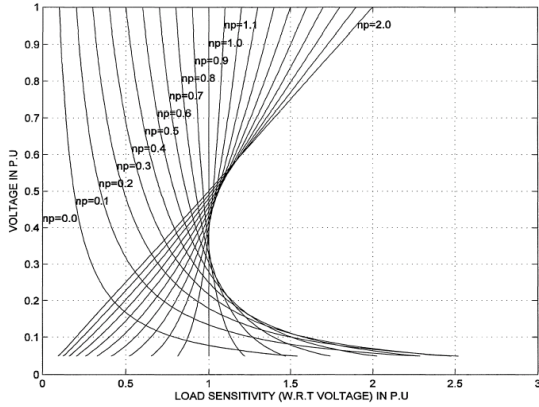
Fig. 5c. Voltage Dependent Load Sensitivity vs Voltage for varying Indices
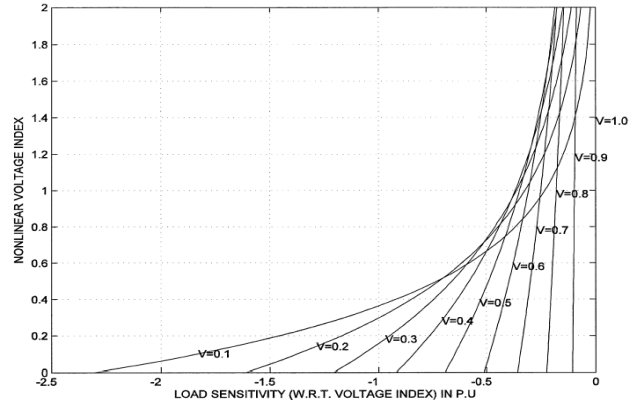

Fig.5d. Voltage Dependent Load Sensitivity (w.r.t Index) vs Indices for varying Voltages
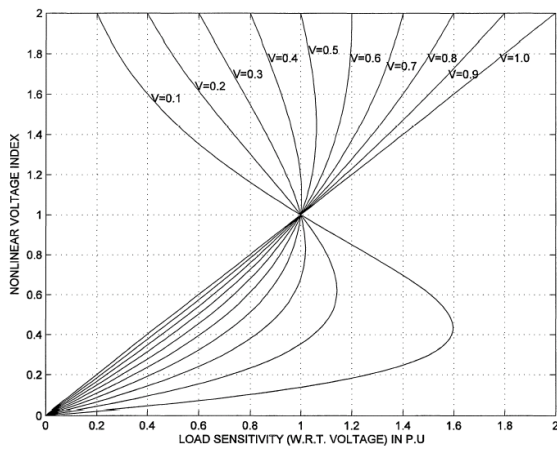

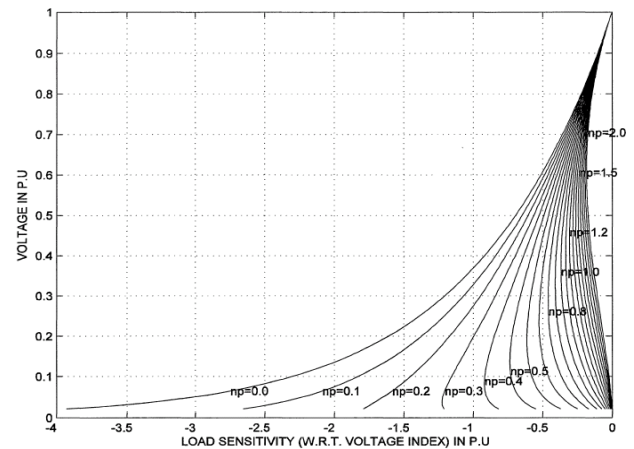Fig. 5e. Voltage dependent Load Sensitivity (w.r.t voltage) vs Indices for varying Voltage

Fig.5f. Voltage Dependent Load Sensitivity vs Voltage for varying exponents

$$\frac{\partial^2 P_{L_i}}{\partial np_i . \partial V_i} = \frac{P_{0_i}}{V_{0_i}^{np_i}} V_i^{np_i - 1} + np_i \frac{P_{0_i}}{V^{np_i}} V_i^{np_i - 1} \ln\left(\frac{V_i}{V_{0_i}}\right)$$

$$= \frac{P_{0_i}}{V_{0_i}^{np_i}} V_i^{np_i - 1} \left(1 + np_i \ln\left(\frac{V_i}{V_{0_i}}\right)\right) > 0 \qquad (6.5)$$

or

$$1 + np_i \ln\left(\frac{V_i}{V_{0_i}}\right) > 0 \quad \Rightarrow \quad \ln\left(\frac{V_i}{V_{0_i}}\right) > -\frac{1}{np_i}$$

or

$$V_i > V_{0_i} \varepsilon^{\left(-\frac{1}{np_i}\right)} \qquad (6.6)$$

The load-voltage sensitivity is a constantly increasing function for $V > 0$ if $np_i = 0$, $V > 0.3679 \, V_0$ for $np_i = 1$ and $V > 0.6065 \, V_0$ if $np_i = 2$. I other words a positive change in voltage index np_i (due to a change in the aggregation of loads) brings about a positive change in the voltage sensitivity of load approximated by the exponential load model. Figs. 5(c)-(f) show the behaviour of these sensitivities for $V_{0_i} = 1 p.u$, $P_0 = 1 p.u$ (normalized load constants).

VII.   ROLE OF GENERATOR MODELS IN ISOLATING BIFURCATION POINTS

The real power at load bus 5 in the WSCC system is chosen as the critical parameter for the system represented by each of the models (a)-(d) in section 5. The bifurcation analysis yields the results as shown in Table 2 for constant power case $np_i = nq_i = 0$. The modal behaviour of each of these models is as shown in Fig. 6(a)-(b). JLF denotes the Jacobian of the network equations with respect to the network variables and JAE,

the Jacobian of the stator and network equations with respect to all the algebraic variables: network variables and the stator currents. It is seen that in model (b) and (c) with fast exciters, another pair of eigenvalues joins the critical pair in the left half plane. This second pair is associated with the rotor variables of the second generator (δ_2, ω_2). They follow the movement of the critical pair and move back into the left half plane after the critical pair have split along the real axis, point B, in Fig. 6(b). The movement of both these pairs are captured in Table 3 as the real power at bus 5 is increased.

TABLE 2.1 Modal Behaviour of Model (a) for different Loads

Load at Bus 5	Sign(det JLF)	Sign(det JAE)	Critical Eigenvalue(s)	Associated States
4.3	+	+	$-0.1433 \pm j2.0188$	$E'_{q1} \& R_{f1}$
4.4	+	+	$0.0057 \pm j2.2434$	$E'_{q1} \& R_{f1}$
4.5	+	+	$0.3400 \pm j2.5538$	$E'_{q1} \& R_{f1}$
4.6	+	+	$1.1350 \pm j2.8016$	$E'_{q1} \& R_{f1}$
4.7	+	+	$2.5961 \pm j2.2768$	$E'_{q1} \& R_{f1}$
4.8	+	+	$9.2464, 1.8176$	$\delta_2 \& \omega_2, E'_{q1} \& R_{f1}$
4.9	+	-	1.0542	$E'_{q1} \& R_{f1}$
5.0	+	-	0.6298	$E'_{q1} \& R_{f1}$
5.1	+	-	0.2463	$E'_{q1} \& R_{f1}$
5.15	+	-	-0.6832	$E'_{q1} \& R_{f1}$
5.2	Load Flow does not converge			

TABLE 2.2 Modal Behaviour of Model (b) for different loads

Load at Bus 5	Sign(det JLF)	Sign(det JAE)	Critical Eigenvalue(s)	Associated States
4.4	+	+	$-0.0957 \pm j0.1407$	$\delta_2 \& \omega_2$
4.5	+	+	$0.0308 \pm j10.0034$	$\delta_2 \& \omega_2$
4.6	+	+	$0.3802 \pm j9.9008$	$\delta_2 \& \omega_2$
4.7	+	+	$0.9344 \pm j10.1111$	$\delta_2 \& \omega_2$
4.8	+	+	$1.3907 \pm j11.1963$	$\delta_2 \& \omega_2$
4.9	+	-	$24.4174, 0.1104 \pm j11.3605$	$E'_{q1} \& E_{fd1}, \delta_2 \& \omega_2$
5.0	+	-	6.0978	$E'_{q1} \& E_{fd1}$
5.1	+	-	2.5680	$E'_{q1} \& E_{fd1}$
5.15	+	-	0.5417	$E'_{q1} \& E_{fd1}$
5.2	Load Flow does not converge			

TABLE 2.3 Modal Behaviour of Model (c) for different Loads

Load at Bus 5	Sign(det JLF)	Sign(det JAE)	Critical Eigenvalue(s)	Associated States
4.2	+	+	$-0.0048 \pm j7.4848$	$\delta_2 \& \omega_2$
4.3	+	+	$0.2522 \pm j7.4248$	$\delta_2 \& \omega_2$
4.4	+	+	$0.5333 \pm j7.4024$	$\delta_2 \& \omega_2$
4.5	+	+	$0.8574 \pm j7.4233$	$\delta_2 \& \omega_2$
4.6	+	+	$1.2592 \pm j7.5151$	$\delta_2 \& \omega_2$
4.7	+	+	$1.8164 \pm j7.7697$	$\delta_2 \& \omega_2$
4.8	+	+	$2.7800 \pm j8.6826$	$\delta_2 \& \omega_2$
4.9	+	-	$12.2699, 0.4398 \pm j10.0051$	$E'_{q1} \& E_{fd1}, \delta_2 \& \omega_2$
5.0	+	-	$4.1693, 0.1100 \pm j9.3208$	$E'_{q1} \& E_{fd1}, \delta_2 \& \omega_2$
5.1	+	-	1.6687	$E'_{q1} \& E_{fd1}$
5.15	+	-	0.0369	$\delta_1 \& \delta_2$
5.2	Load Flow does not converge			

TABLE 2.4 Modal Behaviour of Model (d) for different loads

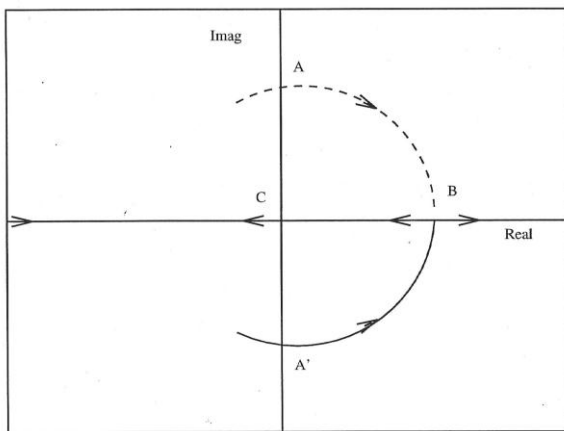| Load at Bus 5	Sign(det JLF)	Sign(det JAE)	Critical Eigenvalue(s)	Associated States
4.4	+	+	$-0.2388 \pm j1.6434$	E'_{q1} & R_{f1}
4.5	+	+	$-0.1997 \pm j1.7778$	E'_{q1} & R_{f1}
4.6	+	+	$-0.1265 \pm j1.9985$	E'_{q1} & R_{f1}
4.7	+	+	$0.0614 \pm j2.4531$	E'_{q1} & R_{f1}
4.8	+	+	$1.7612 \pm j3.9016$	E'_{q1} & R_{f1}
4.9	+	-	1.8483	E'_{q1} & R_{f1}
5.0	+	-	0.9059	E'_{q1} & R_{f1}
5.1	+	-	0.3726	E'_{q1} & R_{f1}
5.15	+	-	-0.0424	E'_{q1}, δ_1 & R_{f2}
5.2	Load Flow does not converge			

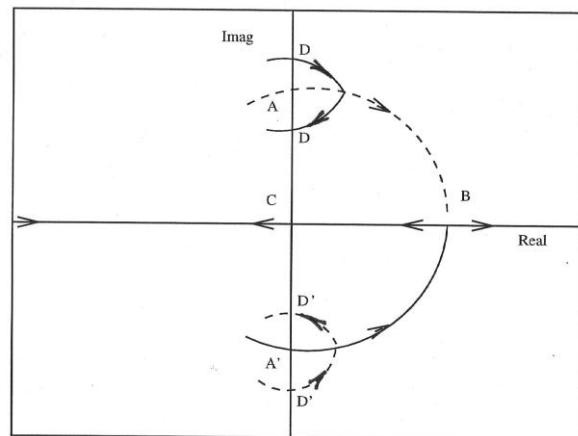Fig 6 (a) Critical Eigenvalue pair movement for Models (a) and (d)

Fig 6(b) Critical eigenvalues movement for Models (b) and (c)

TABLE 3. Modal Behaviour of Model (b) for increasing load at bus 5 for Ka=50

Load at Bus 5	Sign(det JLF)	Sign(det JAE)	Critical Eigenvalue(s)	Associated States
4.80	+	+	$1.3907 \pm j11.1963$	δ_2, ω_2
4.82	+	+	$0.0443 \pm j15.5037$	δ_2, ω_2
4.84	+	+	$0.5983 \pm j11.7688$	δ_2, ω_2
4.86	+	+	$0.3174 \pm j11.5990$	δ_2, ω_2
4.88	+	+	$0.1862 \pm j11.4621$	δ_2, ω_2
4.90	+	-	$24.4175, 0.1105 \pm j11.3605$	E_{q1}, E_{fd1}
4.92	+	-	$14.0688, 0.0611 \pm j11.2824$	E_{q1}, E_{fd1}
4.94	+	-	$10.5866, 0.0265 \pm j11.2200$	E_{q1}, E_{fd1}
4.96	+	-	$8.5713, 0.0010 \pm j11.1686$	E_{q1}, E_{fd1}
4.98	+	-	7.1711	E_{q1}, E_{fd1}
5.00	+	-	6.0978	E_{q1}, E_{fd1}
5.02	+	-	5.2207	E_{q1}, E_{fd1}
5.04	+	-	4.4687	E_{q1}, E_{fd1}
5.06	+	-	3.7973	E_{q1}, E_{fd1}
5.08	+	-	3.1738	E_{q1}, E_{fd1}

VIII.   EFFECT OF NONLINEARITY OF LOAD MODELS ON BIFURCATIONS

Table 4 depicts the effect of nonlinear load indices on Hopf bifurcation points for different generator models chosen for each value of critical loading parameter, the real power at bus 5. The AVR gain Ka is chosen as 25. It is seen that the flux decay model (neglecting damper winding dynamics) essentially makes the system more stable and Hopf bifurcations occur at a later stage. The type of exciter model used also has some influence on the bifurcation point; model (c), which is a flux decay model coupled with a fast exciter, undergoes Hopf Bifurcations at a much later stage than the other models.

TABLE 4 Effect of Nonlinearity of Loads on Bifurcation Points of Different Models

Load Index	Load (in p.u) at Bus 5 at corresponding Hopf Bifurcation Point			
	Model (a)	Model (b)	Model (c)	Model (d)
0.0	4.4	4.6	4.4	4.7
0.1	4.55	4.7	4.5	4.8
0.2	4.65	4.8	4.6	4.95
0.5	5.05	5.1	4.95	5.15
0.6	-	-	5.05	-
0.7	-	-	5.10	-
0.8	-	-	5.15	-
0.9	-	-	-	-

IX.   EFFECT OF EXCITER GAIN

The exciter gain Ka (assumed same for all machines in the system) also has some influence on the onset of Hopf bifurcations essentially prolonging their occurrence for higher values as shown in Fig. 7 for model (a).
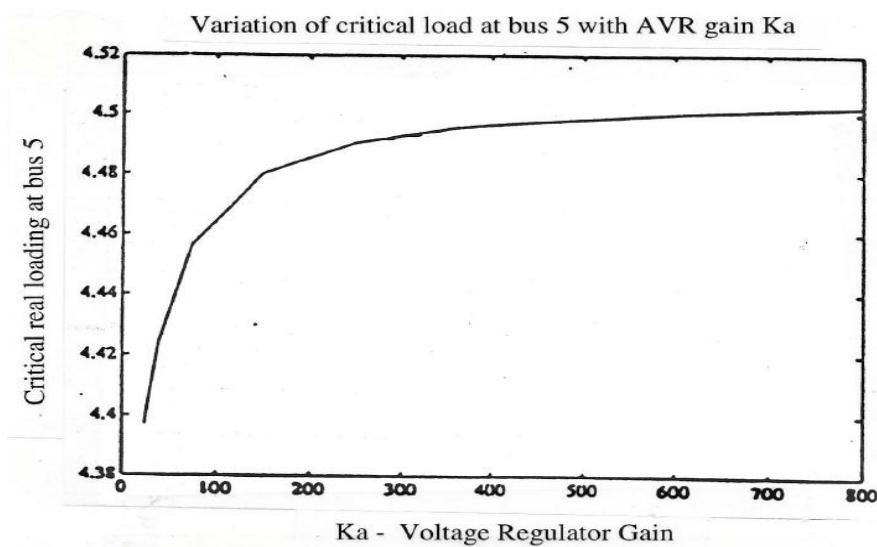

Fig. 7 Effect of Regulator Gain Ka on bifurcation point

X.   CONCLUSIONS

Power voltage relationships in power systems were investigated. The effect of different generator models in defining stability of multimachine systems were dealt upon using power voltage relationships at a critical load bus. The effect of nonlinear voltage dependent load characteristics on system stability and the onset of bifurcations was shown as also the effect of AVR gain. Further work is needed to fully understand power voltage relationships and the occurrence of dynamic phenomena apart from simple Hopf Bifurcations, for example, period doubling bifurcations and chaos, in large power systems.

REFERENCES

[1] J. Guckenheimer and P.Holmes, Nonlinear Oscillations, Dynamical Systems and Bifurcations of vector fields,' *Applied mathematical Sciences* 42, Springer-Verlag, 1983.

[2] V. Ajjarapu and B.Lee, 'Bifurcation theory and its application to nonlinear dynamical phenomena in an electric power system,' *IEEE Transactions on Power Systems*, vol 7, No.1, February 1992, pp 424-431.

[3] P.W.Sauer, B.C. Lesieutre and M.A.Pai, ' Dynamic vs Static aspects of voltage problems,' *Bulk Power System Voltage Phenomena, voltage stability and security, International Workshop*, Deep Creek Lake, Maryland, Aug 4-7, 1991.

[4] C.Rajagopalan, B.Lesieutre, P.W.Sauer and M.A.Pai, 'Dynamic Aspects of Voltage/Power characteristics,' *IEEE Transactions on Power Systems*, vol 7, No. 3, August 1992, pp 990-1000.

[5] M.A.Pai, P.W.Sauer, B.C. Lesieutre and A.Adapa, 'Structural Stability in Power Systems- Effect of Load Models,' *IEEE Transactions on Power Systems*, Vol. 10, No. 2, May 1995, pp 609-615.

[6] EPRI Final Report, 'Power System Dynamic Analysis,' Phase I, EL 484, Project 670-1, July 1977.

[7] EPRI Final Report EL-850, Project 849-1, 'Determining Load Characteristics for Transient Performance,' Vol 1-4, prepared by General Electric Company, Schenectady, New York, March 1981.

[8] EPRI Final Report EL-5003, Project 849-7, 'Load Modeling for Power flow and Transient Stability computer services,' Vol 1 and 2, prepared by General Electric Company, Schenectady, New York, Jan 1987.

[9] B.C. Lesieutre, P.W. Sauer and M.A.Pai, 'Sufficient conditions on static load models for network solvability,' *Proceedings of the Twenty-Fourth Annual North American Power Symposium*, Reno, NV, Oct 5-6, 1992, pp 262-271.

[10] C.Concordia and S.Ihara, 'Load representation in power system stability studies,' *IEEE Trans. On PAS*, vol-101, No 4, April 1982, pp 969-977.

[11] IEEE Task Force on load representation for dynamic performance, 'Load representation for dynamic performance analysis,' *IEEE Trans. On Power Systems*, PWRS-8, No.2, May 1993, pp 472-481.

[12] IEEE Task force on load representation for Dynamic performance, 'Standard Load Models for Power Flow and Dynamic Performance Simulation,' *IEEE Trans. On Power Systems*, vol-10, No 3, Aug 1995, pp 1302-1313.

[13] S.R. Fernandes, P.W Sauer and M.A. Pai, 'Quantification of Parameter Importance in Power Systems Steady State Stability Analysis,' *Proceedings of the 28th North American Power Symposium*, Massachussetts Institute of Technology, Cambridge, MA, USA, November 10-12, 1996, pp. 133-138.

[14] S.R. Fernandes, 'Generalized Extension of AESOPS and PEALS Algorithms for Sensitivity Analysis,' *Journal of the Institution of Engineers*, Singapore, vol 45, Issue 1, 2005, pp. 14-37.

APPENDIX A

R_S	X_d	X_q	X_d'	X_q'	T_{d0}'
0.00185p.u	1.942p.u	1.921p.u	0.330p.u	0.507p.u	5.330p.u
T_{q0}'	H	D	X_e	K_A	T_A
0.593 s	2.8323 s	0.0 p.u	0.5	50	0.02
K_E	T_E	K_F	T_F	A_{ex}	B_{ex}
1.0	0.78	0.01	1.2	0.397	0.09
$V_{r\max}$	$V_{r\min}$	T_{RH}	K_{HP}	T_{CH}	T_{SV}
9.9	-8.9	10.0	0.26	0.5	0.2